SLAC–PUB–7458
April 1997

Bunch Compression for an FEL at NLCTA*

Frank Zimmermann
Stanford Linear Accelerator Center
Stanford University, Stanford, CA 94309, USA

As part of the design effort for a free electron laser driven by the Next Linear Collider Test Accelerator (NLCTA), I report studies of bunch-length compression utilizing the existing infrastructure and hardware. In one possible version of the NLCTA FEL, bunches with 900-μm FWHM length, generated by an S-band photo-injector, would be compressed to an rms length of 60–120 μm before entering the FEL undulator. It is shown that, using the present magnetic chicane, the bunch compression is essentially straightforward, and that almost all emittance-diluting effects, *e.g.* wakefields, chromaticity, or space charge in the bending magnets, are small. The only exception to this finding is the predicted increase of the horizontal emittance due to coherent synchrotron radiation (CSR). Estimates based on existing theories of coherent synchrotron radiation suggest a tripling or quadrupling of the initial emittance, which seems to preclude bunch compression during regular FEL operation. Serendipitously, the magnitude of the predicted emittance growth would, on the other hand, make the NLCTA chicane an excellent tool for measuring the effects of coherent synchrotron radiation. This will be of considerable interest to many future projects, in particular to the Linac Coherent Light Source (LCLS).
As an aside, it is shown that coherent synchrotron radiation in a bending magnet gives rise to a minimum possible bunch length, which is very reminiscent of the Oide limit on the vertical spot size at the interaction point of a linear collider.

(Submitted for Publication)

*Work supported by the US Department of Energy under contract DE–AC03–76SF00515.

1 Introduction

The Next Linear Collider Test Accelerator (NLCTA) [2] is a prototype high-gradient X-band linac, designed to study multi-bunch beam handling and X-band rf systems for the Next Linear Collider (NLC). It is presently under investigation to use the NLCTA as a test bed for the Linac Coherent Light Source [3], *i.e.*, for studies of self-amplified spontaneous emission (SASE), coherent synchrotron radiation and emittance preservation [4]. Moreover, it is being contemplated to convert the NLCTA into a dedicated FEL user facility in the medium or long term [4]. In order to generate a high peak current to study SASE with reasonable FEL gain and saturation lengths, the bunch length in the FEL undulator should be about 2–3 times shorter than what is delivered by S-band photoinjectors. One possible solution is to compress the bunch after it has been accelerated to about 100 MeV.

In this report, we discuss a bunch-compression scheme utilizing the existing NLCTA chicane. We describe the longitudinal distributions and the transverse emittance growth due to coherent synchrotron radiation, space-charge effects and wake fields, that can be expected in such a scheme. We also give a rough estimate of the structure alignment tolerances. and we derive an expression for the minimum bunch length at the exit of a bending magnet due to CSR. Finally, we will draw some conclusions.

A state-of-the-art S-band photoinjector delivers electron bunches with a 1-nC charge, an FWHM bunch length of 900 μm (with 90 μm full rise and fall time), a beam energy of 6 MeV, an initial energy spread of about 0.1%, and, most importantly, an initial normalized horizontal and vertical emittance of 1.5 mm mrad. In the following, we assume that such a photoinjector is in place and use the above values as initial beam parameters in our studies of NLCTA-FEL beam dynamics.

To ensure the transverse coherence of the radiation, a small transverse emittance is required in the undulator:

$$\gamma\epsilon_{x,y} < \frac{\gamma\lambda}{4\pi} \approx 5 \text{ mm mrad}, \tag{1}$$

where the value on the far right side applies to a radiation wavelength of $\lambda = 100$ nm and a beam energy of 325 MeV. Our study goal was to compress the bunch length by a factor of 3 or 4, while maintaining a transverse normalized emittance that is smaller than 2 mm mrad and an rms energy spread not much larger than 0.15% (indeed an energy spread below 0.02% could be achieved).

Since the studies reported here were conducted, plans to compress the bunches with a magnetic chicane have diminished, and, instead, the construction and use of a novel multi-cell X-band rf gun is now being proposed [5]. The beam parameters assumed for the X-band gun are about the same as for the S-band rf gun, except for a shorter bunch length, which will render bunch compression unnecessary. For the routine FEL operation, the chicane will be bypassed by a straight beam pipe. However, the chicane will be left in place and could be used for dedicated experiments on coherent synchrotron radiation in a bunch compressor.

2 Bunch Compression

If a bunch with a nonzero correlation of energy and longitudinal position ('δ-z') is transported through a beam line with energy-dependent path length, *i.e.*, with a nonzero r_{56} matrix-element [6], the bunch is either compressed or expanded.

In linear approximation, the final bunch length at the end of the beam line is given by

$$\sigma_{zf}^2 = \sigma_{zi}^2(1 + r_{56}f)^2 + \sigma_{\delta i}^2 r_{56}^2 \tag{2}$$

where σ_{zf} and σ_{zi} are the final and initial bunch lengths, respectively, $\sigma_{\delta i}$ the initial relative energy spread, and

$$f \equiv \frac{d\delta}{dz} = -\frac{eVk\sin\psi}{E_0 + eV\cos\psi} \approx -k\tan\psi \tag{3}$$

denotes the magnitude of the δ-z correlation. Here, the term E_0 is the initial beam energy, V the accelerating voltage, e the electron charge, and $k \equiv 2\pi/\lambda$ the rf wave number. On the right-hand side of Eq. (3), we have assumed that the δ-z correlation is introduced by the rf wave, with the rf off-crest (rf phase $\psi \neq 0$). To first order, this is a good approximation. A more refined expression would include a contribution from beam loading and longitudinal wakefields.

The NLCTA accommodates a magnetic chicane located after the injector at a beam energy of about 100 MeV. The chicane consists of 4 bending magnets and 12 quadrupoles. The quadrupoles can be used to change the energy-dependent path length. Figure 1 presents a schematic of the NLCTA chicane, in which the 12 quadrupoles used for adjusting the r_{56} are marked in black.

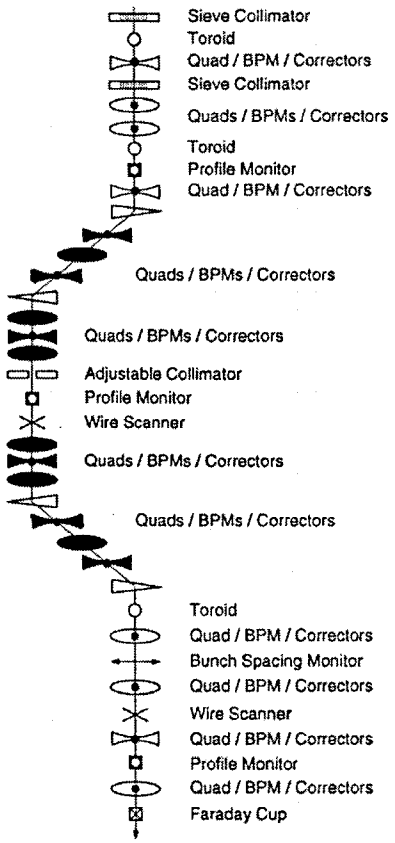

Figure 1: NLCTA chicane. Quadrupoles used for r_{56} adjustment are shown in black.

To reduce the rms bunch length from initially 260 μm to $\sigma_{zf} \approx 60$–120 μm, we need to choose the rf phase, rf voltage and the r_{56} of the chicane such that $(1 + r_{56}f) \approx 0.23$–$0.45$. In simulations using the longitudinal-tracking code LITRACK [7] and the six-dimensional program MAD [8], we have varied the two parameters r_{56} and f over a wide range of values, while keeping the final bunch length constant. We found that about the best performance is obtained for $r_{56} \approx -20$ mm, where the negative sign indicates that the chicane functions like an arc where higher-energetic particles advance more slowly. For this value of r_{56} and an initial energy spread of $\sigma_{\delta 0} \approx 0.1\%$, the last term in Eq. (2), $r_{56}\sigma_{\delta 0}$, is insignificant.

It is advantageous to operate the chicance as an 'arc' (with $r_{56} < 0$), because in that case the second-order momentum compaction factor and the curvature of the rf voltage partially cancel each other, while in the opposite case of a real 'chicane' ($r_{56} > 0$) these two nonlinear terms would add. In the next section, we will show that, furthermore, for an r_{56} value around -20 mm the emittance growth caused by coherent synchrotron radiation is minimum.

In Fig. 2, the design optics of the NLCTA is shown. Figure 3 depicts a modified optics where the six quadrupoles in the chicane were adjusted in strength to yield $r_{56} = -20$ mm. In the latter case, the beta functions in the chicane are larger, and, as a consequence, the chromatic emittance growth through the chicane is slightly enhanced compared with the design.

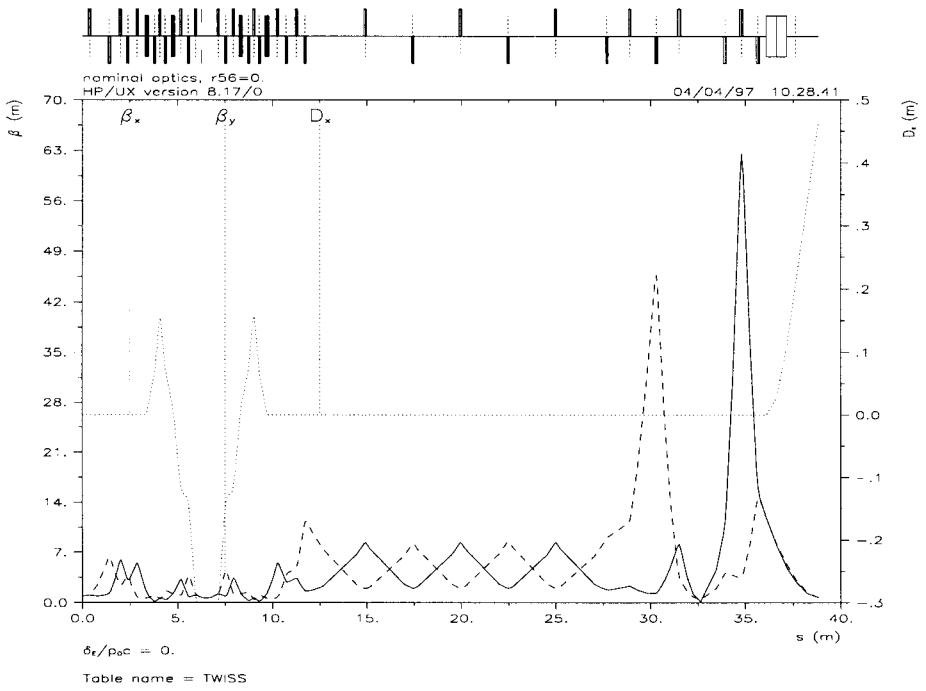

Figure 2: Nominal NLCTA optics ($r_{56} = 0$ mm, $t_{566} = -0.535$ m). Beta functions and dispersion.

Figure 4 shows a typical simulation result with LITRACK (which includes the curvature of the RF, the r_{56} and t_{566} matrix elements *i.e.*, first and second order momentum compaction, and the short-range wake field). Table 1 summarizes simulation results for three different final energies and bunch lengths.

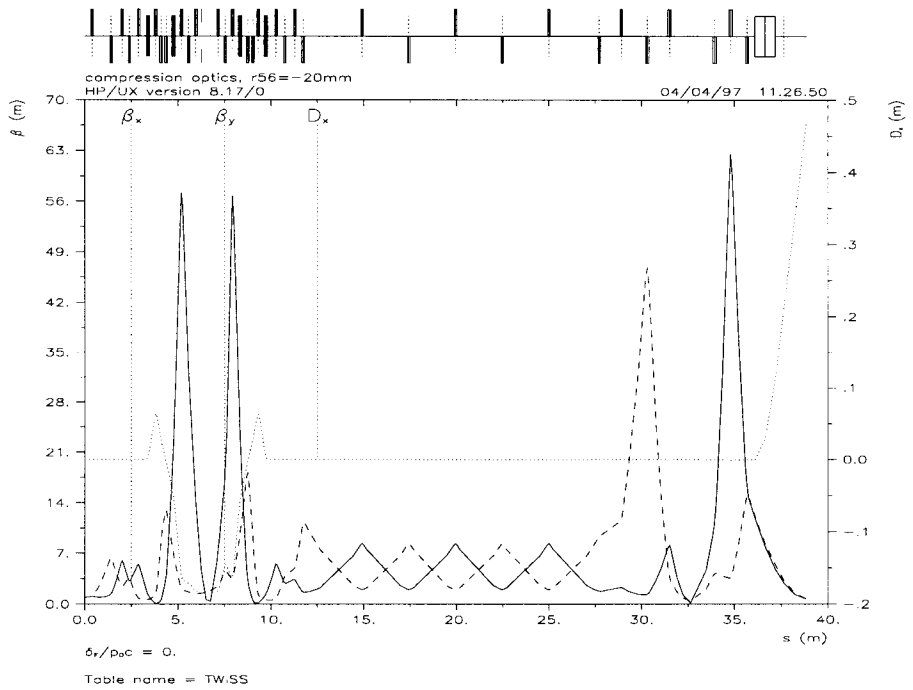

Figure 3: NLCTA optics with $r_{56} = -20$ mm ($t_{566} = -0.167$ m). Beta functions and dispersion.

version	I	II	III
beam energy [MeV]	102	205	325
rms bunch length [μm]	120	80	60
rms energy spread [%]	0.73	0.33	0.20
bunch charge [nC]	1	1	1
peak current [kA]	1	1.5	2

Table 1: Beam parameters achieved in longitudinal simulations of the compression and acceleration process, using the code LITRACK [7].

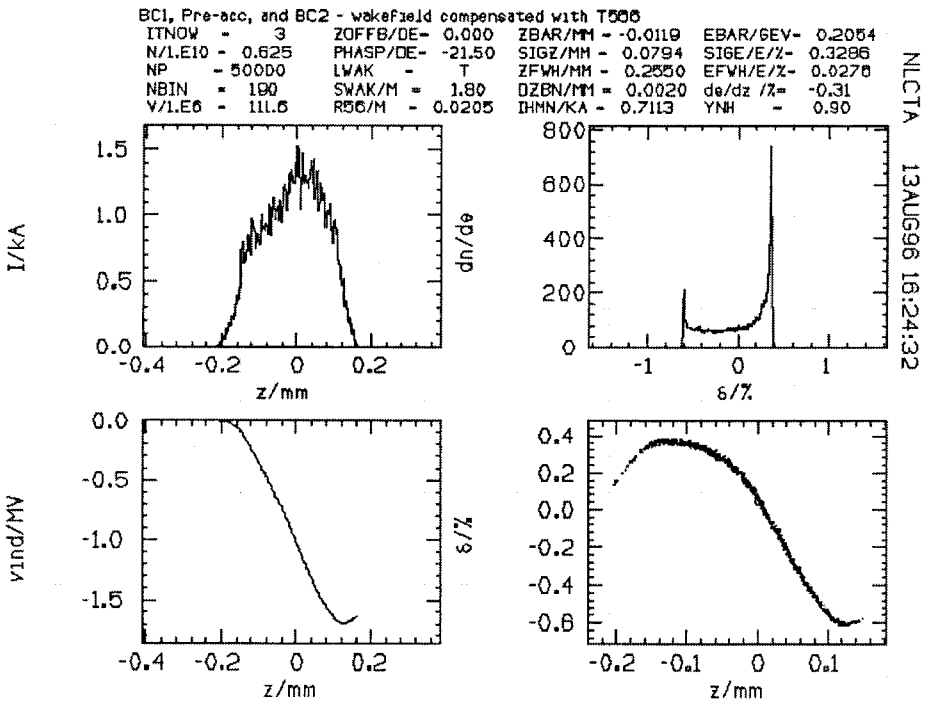

Figure 4: Longitudinal beam distribution after compression, for a final bunch length of 80 μm at 205 MeV. Top left: current vs. position: top right: energy distribution; bottom left: beam-induced wakefield in the accelerator section; bottom right: distribution of energy vs. position.

In addition to longitudinal LITRACK simulations, the full six-dimensional beam dynamics was studied using a modified version of the program MAD [8]. Figure 5 a–c display the evolution of all three beam sizes during the compression process, for a final bunch length of 60 μm.

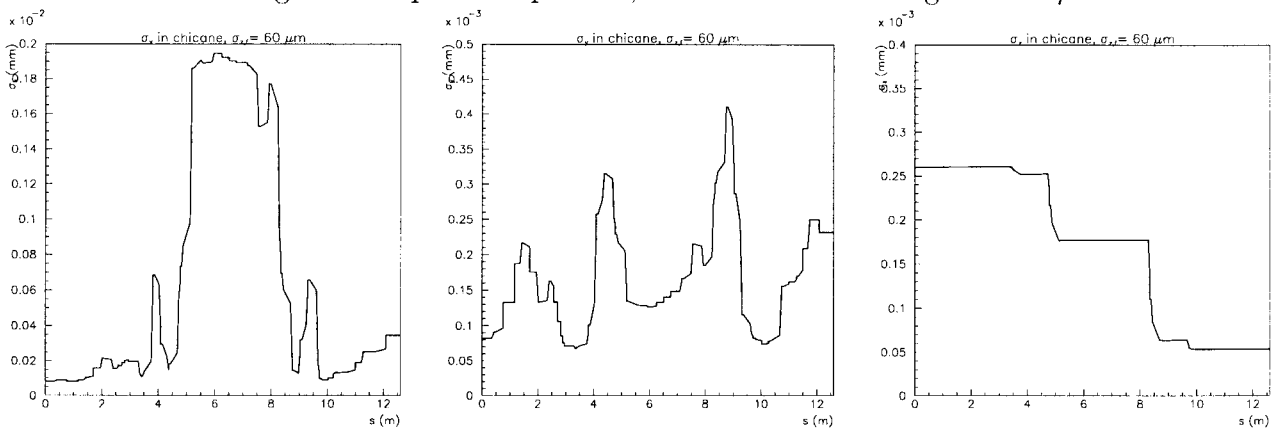

Figure 5: Beam-size changes in the NLCTA chicane, as the bunch is compressed to $\sigma_{zf} \approx 60$ μm. Left: σ_x, center: σ_y, right: σ_z.

In the six-dimensional simulation, an initial horizontal emittance of $\gamma\epsilon_x \approx 1.5$ mm mrad increases to 2.1 mm mrad for the design optics with $r_{56} = 0$ mm and the same rf phase as for compression. This emittance increase is dominated by second-order dispersion. For $r_{56} = -20$ mm, the horizontal emittance increases even more, to about 2.7 mm mrad, because of the enhanced horizontal chromaticity. In both cases the normalized vertical emittance stays constant at 1.5 mm mrad.

At this point, we can conclude that it is easy to achieve the bunch length, energy spread, peak current, and vertical emittance desired for a 100-nm SASE FEL, assuming nothing but a state-of-the-art rf gun performance. However, as we will show in the next section, it is possible that the horizontal emittance increases substantially due to coherent synchrotron radiation in the chicane.

3 Coherent Synchrotron Radiation

For intense short bunches, coherent synchrotron radiation (CSR) can lead to an enhanced energy spread and to increased emittance growth. The effect of coherent synchrotron radiation has recently been studied by various authors [9, 10, 11, 12].

According to Ref. [9], the rms energy spread induced by coherent synchrotron radiation in a bending magnet of radius R and length L_d is approximately

$$\delta_{rms}^{CSR} \approx 0.2 \, \frac{N r_e L_d}{\gamma R^{2/3} \sigma_z^{4/3}} \tag{4}$$

where N is the number of particles in the bunch, γ the Lorentz factor, r_e the classical electron radius, and σ_z the rms bunch length. Using the NCLTA parameters $N \approx 6.3 \times 10^9$, $L_d = 0.2$ m, $R = 1.2$ m,$\gamma = 190$, $\sigma_{zf} \approx 60$ μm, we find

$$\delta_{rms}^{CSR} \approx \begin{cases} 1.4 \times 10^{-3} & \text{for } \sigma_z = 60 \ \mu\text{m} \\ 5.5 \times 10^{-4} & \text{for } \sigma_z = 120 \ \mu\text{m} \end{cases} \tag{5}$$

r_{56}	$\Delta(\gamma\epsilon_x)$
+70 mm	3.9 μm
+20 mm	0.9 μm
0 mm	0.8 μm
−20 mm	0.3 μm
−70 mm	2.1 μm

Table 2: Rough estimate of emittance growth due to CSR in last bending magnet for $\sigma_{zf} \approx 120$ μm.

For a final bunch length of 120 μm, we can estimate the emittance growth due to CSR occuring in the last bending magnet by

$$\Delta(\gamma\epsilon_x) \approx \gamma(\sigma_x\eta_x' + \sigma_x'\eta_x)\ \delta_{rms}^{CSR}. \tag{6}$$

Table 2 lists, for 5 different values of r_{56}, the emittance growth estimated according to Eq. (6).

To study the effect of coherent synchrotron radiation on the horizontal emittance, we have performed a series of six-dimensional simulations, using a modified version of the program MAD [8, 22]. In these simulations, at the center of each bending magnet the energy of a particle was varied as a function of its longitudinal position, using the overtake 'wake' function derived in Ref. [9].

Figure 6 a and b show exemplary simulation results of the coherent-synchrotron radiation effect in the longitudinal phase space. It is somewhat surprising that the distribution becomes fuzzier when coherent synchrotron radiation is turned on in the simulation. This can be explained by a fairly large chromaticity and nonzero t_{116} and t_{126} matrix elements between the bending magnets and the end of the beam line, which couples the horizontal motion into the longitudinal. That the 'fuzziness' is related to the horizontal emittance (as it should if it is due to chromaticity) was confirmed in the simulations.

The simulated final horizontal emittance is depicted as a function of the initial emittance for a bunch compression to 120 μm and 60 μm in Fig. 7 and Fig. 8, respectively. Each figure shows 3 curves, representing the three cases of no coherent synchrotron radiation, coherent synchrotron radiation according to Eq. (4), and coherent synchrotron radiation with reduced apertures (half apertures of 1.5 and 1 mm) in the last two bending magnets.

For the expected initial emittance of 1.5 mm mrad, the projected final emittance is of the order 8–11 mm mrad. When the aperture of the last two bending magnets is reduced, a final emittance of about 5 mm mrad can be achieved. This may be barely acceptable for FEL operation; compare Eq. (1).

A striking feature of Figs. 7 and 8 is the substantial emittance growth already present without coherent synchrotron radiation. The source of this emittance increase was investigated by comparing the emittance growth for two different values of the rms energy spread and for two different values of the r_{56}. The results of MAD tracking simulations are presented in Fig. 9. They confirm the statement made earlier that the emittance growth for $r_{56} = 0$ is dominated by dispersion, while that for $r_{56} = -20$ mm is essentially due to chromaticity.

Since the growth of the projected emittance is so large, we investigate in more detail

- the effect of shielding,
- the emittance growth of the slice emittance,

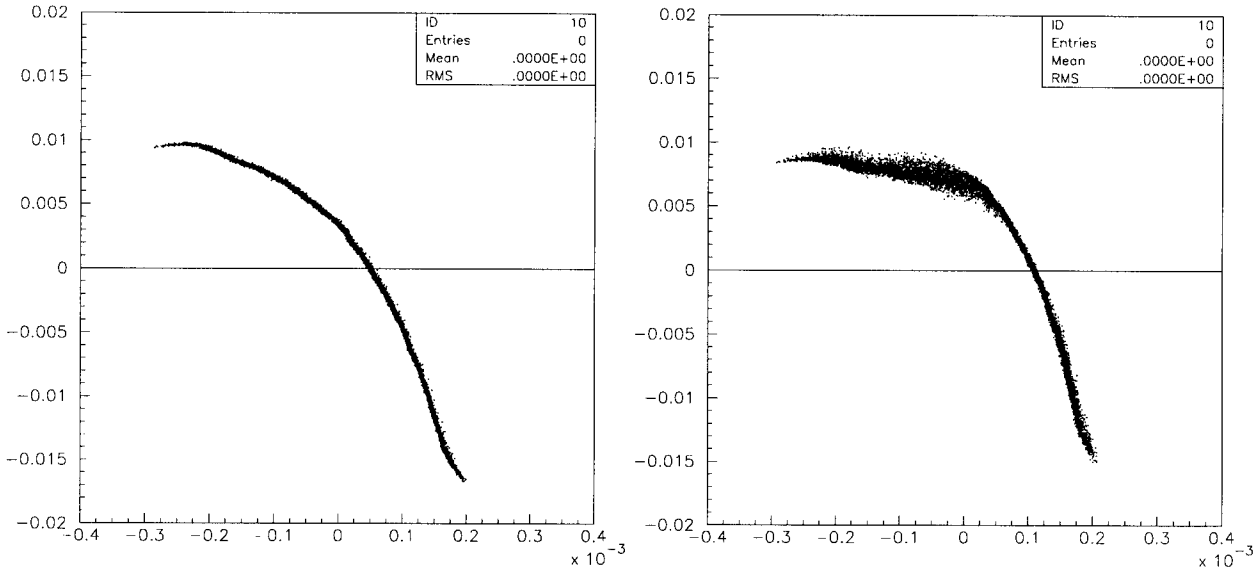

Figure 6: Longitudinal beam distribution after compression for a final bunch length of 60 μm, as obtained by a 6-dimensional simulation. Plotted is the energy deviation versus the longitudinal position (in meter). Left: without coherent synchrotron radiation; right: coherent synchrotron radiation included. The fuzzy appearance is caused by coupling from the horizontal motion via the chromaticity.

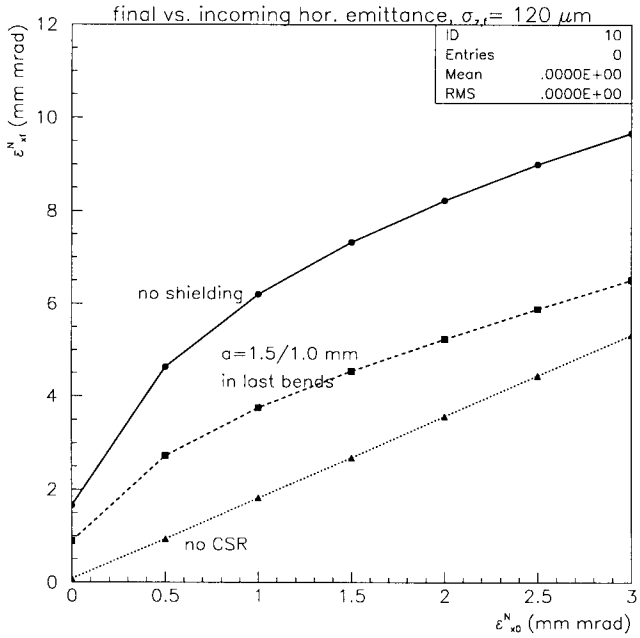

Figure 7: Final versus incoming normalized horizontal emittance for a final rms bunch length of 120 μm, and considering the three cases without CSR, with nominal CSR, and with reduced apertures in the last two bending magnets.

- other mitigations, e.g., additional sextupoles, and
- the applicability of the theory.

We will successively address each of these 4 items.

Effect of Shielding

When the full aperture h is smaller than the critical aperture

$$h_{crit} \equiv (\pi \sigma_z \sqrt{R})^{2/3} \tag{7}$$

the shielding by the vacuum chamber suppresses the low-frequency synchrotron radiation. In the NLCTA,

$$h_{crit} \approx 3.5 \text{ mm} \ll h \approx 8 \text{ mm} \tag{8}$$

and shielding does not matter, unless the vertical aperture in the bending magnets is decreased to a full aperture less than 3 mm.

By parametrizing coherent-synchrotron radiation wake functions and impedances obtained with Warnock's CSR code [18, 19], Emma derived an empirical relation between the induced energy spread $\delta_{rms}^{CSR}(h)$ and the vacuum-chamber aperture h [17]:

$$\delta_{rms}^{CSR}(h) \approx \left(1 - e^{-\frac{2h}{h_{crit}}+0.8}\right) \delta_{rms}^{CSR}(\infty) \tag{9}$$

where $\delta_{rms}^{CSR}(\infty)$ denotes the induced energy spread without any shielding.

Equation (10) is plotted in Fig. 10. According to the figure, decreasing the full vertical aperture from 15 mm to 2 mm results in a 3 times smaller induced energy spread and correspondingly reduced emittance growth in the last bending magnet.

The Slice Emittance

The argument has been put forward that not the projected emittance but the slice emittance along the bunch is what is relevant for the FEL process. Figure 11 shows the slice emittance along the length of the bunch according to a six-dimensional simulation of the NLCTA-FEL with and without coherent synchrotron radiation, for a final bunch length of 60 μm. Without CSR the normalized slice emittance is equal to the initial emittance of 1.5 mm mrad and the projected emittance is 3.8 mm mrad, increased by chromatic and dispersive effects. When CSR is turned on, the projected emittance increases to about 11 mm mrad, while the slice emittance of 2–2.5 mm mrad is only modestly enhanced from its initial value.

Unfortunately, since the slippage length is comparable to the bunch length, the preservation of the slice emittance may not be too helpful for this particular application.

Other Mitigations

An attempt was made to decrease the chromatic and dispersive emittance growth through the chicane, evident in Fig. 9, by adding two sextupoles (after 1 and 2 thirds of the chicane length). Figure 12 demonstrates that, indeed, with two additional sextupoles the chromatic emittance growth can be significantly reduced.

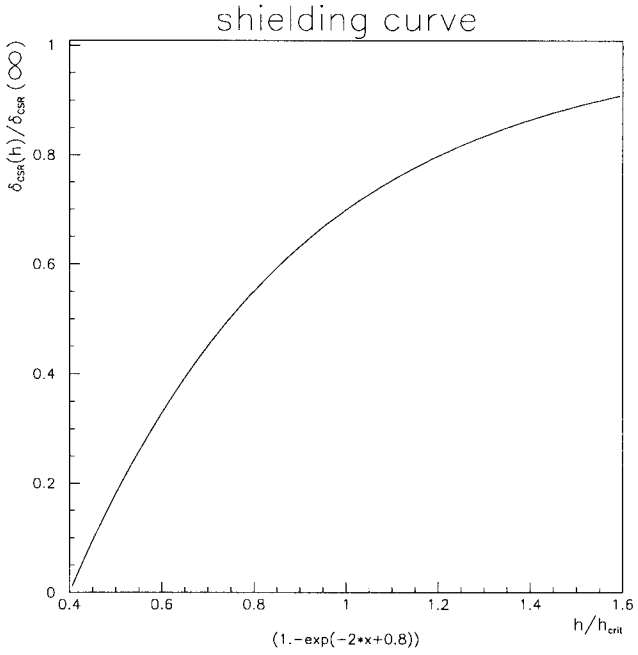

Figure 10: Energy loss suppression factor due to shielding [17].

Unfortunately, as shown in Fig. 13, the optics with additional sextupoles has a much degraded performance when coherent synchrotron radiation is included. Therefore, this optics does not represent an attractive option, unless the theory of coherent synchrotron radiation that we have used considerably overestimates its magnitude (which is possible).

Other Theories of CSR

The theory of coherent synchrotron radiation developed in Ref. [9] only considers motion on a circular orbit, without taking into account the finite length of the bending magnet and the straight orbits before and after the bend. A refined theory which includes the transient effects was proposed in Ref. [11]. The energy loss predicted by this refined theory agrees well with direct numerical solutions of Maxwell's equation as computed with a program by Dohlus and Limberg [13].

In Ref. [11], for later convenience, the bending-magnet length L_d and the bunch length l_b are converted into normalized angles. The normalized bunch length is the solution of a cubic equation:

$$\hat{\phi}_b \equiv \left(12\hat{l}_b + \sqrt{64 + 144\hat{l}_b^2}\right)^{1/2} - \left(-12\hat{l}_b + \sqrt{64 + 144\hat{l}_b^2}\right)^{1/2} \text{ with } \hat{l}_b \equiv \gamma^3 l_b/R \tag{10}$$

where l_b is the FWHM bunch length, and R the bending radius. The normalized bend length is simply

$$\hat{\phi}_m \equiv \gamma\phi_m \tag{11}$$

where, following the convention of Ref. [11], ϕ_m is used to denote the bending angle.

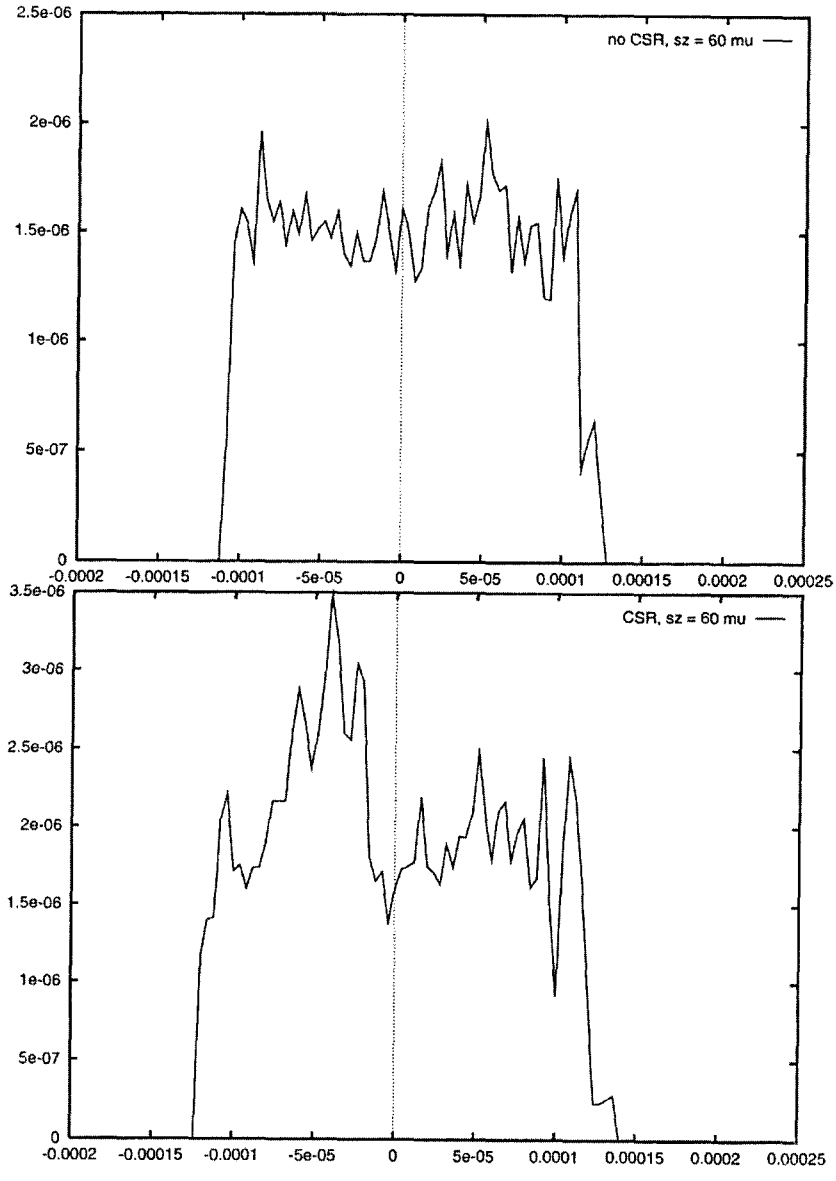

Figure 11: Slice emittance with and without coherent synchrotron radiation as a function of longitudinal position for a final bunch length of 60 μm, as obtained by six-dimensional simulations with the code MAD [8].

The Derbenev formula, Eq. (4), applies in the case $\hat{\phi}_m >> 1$, $\hat{\phi}_b >> 1$, and $\hat{\phi}_b < \hat{\phi}_m$. For NLCTA parameters, using $l_b \approx 700$ μm, we have $\hat{\phi}_m = 34 \ll \hat{\phi}_b \approx 310$, *i.e.*, the bunch is 'longer' than the magnet. Thus, the Derbenev formula is not applicable, and we must calculate instead the induced energy spread predicted for the case of a long bunch (case 4 in Ref. [11]):

$$\delta_{rms}^{CSR} \approx 0.28 \frac{Nr_e}{\sqrt{2\pi}\sigma_z\gamma} \left[4\ln(\gamma\phi_m) - 2\right] \tag{12}$$

For our parameters, this is about twice as large as previously estimated from Eq. (4)!

Nevertheless, both Eq. (4) and Eq. (12) most likely overestimate the real magnitude of the coherent synchrotron radiation considerably, since all these theories are based on a pencil beam and ignore the fact that the horizontal beam size in the chicane is at least a factor of 10 larger than the bunch length. Unfortunately, to our knowledge, so far no theory of coherent synchrotron radiation has been developed which properly includes the transverse beam dimensions.

4 The Minimum Bunch Length

It is interesting to note that the coherent synchrotron radiation gives rise to a minimum achievable bunch length. We first illustrate this for a single NLCTA-style bending magnet. From Ref. [9], the induced energy spread per radian reads

$$\frac{d\delta}{d\alpha} = \frac{0.2Nr_eR^{1/3}}{\gamma\sigma_z^{4/3}} \tag{13}$$

where α is the accumulated bending angle and R the bending angle. The momentum compaction for a single bend is

$$r_{56} = \frac{1}{6}\alpha^3 R \tag{14}$$

and the final bunch lenght is obtained by integrating the product $r_{56}(\alpha' \to \alpha_b)d\delta/d\alpha$ over the bending magnet;

$$\sigma_z \geq \int_0^{\alpha} r_{56}(\alpha' \to \alpha_b)\frac{d\delta}{d\alpha}(\alpha')d\alpha' \approx 0.008\ \alpha_b^4 R^{4/3}\frac{Nr_e}{\gamma\sigma_z^{4/3}} \tag{15}$$

Solving for σ_z yields our estimate of the minimum bunch length behind a single bend

$$\sigma_{z,min}^{bend} \geq \left(0.008\ \frac{\alpha_b^4 R^{4/3} Nr_e}{\gamma}\right)^{3/7} \approx 6\ \mu\text{m} \tag{16}$$

In Fig. 14 we present the final bunch length after a single bending magnet versus the initial one, according to six-dimensional simulations. Results are shown both with and without inclusion of coherent synchrotron radiation. Very clearly, when coherent synchrotron radiation is included, a minimum final bunch length is reached at about the expected value of 6 μm. For shorter incoming bunches, the outgoing bunch length increases dramatically. This behavior is very reminiscent of the Oide effect in linear colliders, where the chromaticity of the focusing lens along with (conventional) synchrotron radiation sets a limit on the minimum achievable IP spot size.

predicts minimum bunch lengths equal to or larger than 10 μm, 24 μm, and 60 μm, respectively. These values are slightly smaller than those obtained in the simulation. The difference could be explained by neglected contributions from the remaining two bends.

5 Space Charge

The emittance growth due to longitudinal and transverse space charge forces in bending magnets was first studied by Talman [14] and by Piwinski [15]. Recently, Carlsten and Raubenheimer [16] have derived the following expression for the emittance growth due to longitudinal space charge:

$$\Delta(\gamma\epsilon_x) = 0.38\ \alpha^2 \frac{\hat{I}}{I_A}\ \ln\left(\frac{\rho_0}{a}\right)\frac{a^2}{\sigma_z} \tag{19}$$

where ρ_0 is the beam pipe radius ($\approx$ 8 mm), $I_A = 17$ kA, $a \approx 2\sqrt{\sigma_z\sigma_y}$ twice the rms beam size, $\sigma_z \approx 120$ μm (or 60 μm) the rms bunch length and α the bend angle (0.17 rad) Evaluating the above formula for the NLCTA parametes (just quoted), one has

$$\Delta(\gamma\epsilon_x) \approx 0.6\ \mu\text{m} \qquad \text{(longit. space charge)} \tag{20}$$

which is the emittance growth due to longitudinal space charge in the last bending magnet for a final bunch length of 120 μm.

In Ref. [16] we also find an expression for the emittance growth due to the transverse space charge:

$$\Delta(\gamma\epsilon_x) \approx 0.14\ \frac{a^{5/2}\alpha_0}{\sqrt{R}\sigma_{zi}}\ln\left(\frac{\rho_0}{a}\right)\frac{I_f}{I_A} \tag{21}$$

where $\alpha_0 = \alpha_f/(1-\sigma_{zf}/\sigma_{zi})$, I_f the final current, and all other variables were defined before. Evaluation yields an emittance growth of

$$\Delta(\gamma\epsilon_x) \approx 0.13\ \mu\text{m} \qquad \text{(transv. space charge)} \tag{22}$$

The emittance increases of Eqs. (6), (19) and (21) all add in quadrature to the initial emittance.

6 Geometric and Resistive-Wall Wakefields

If the aperture in the bending magnets is reduced in order to suppress the coherent synchrotron radiation, resistive-wall and geometric wakefields become a concern. Formulae for the energy loss and for the dipole wakefield may be found, for example, in Refs. [20, 21, 22]. We will use expressions for a round geometry. The wakefield for a flat geometry is, up to a numerical factor of the order one, given by the same formulae, when the beam-pipe radius is replaced by the half aperture $h/2$.

The longitudinal resistive-wall wakefield leads to an average energy loss of

$$\delta_{ave} = \frac{2Nr_e}{\gamma}\ \frac{\Gamma(3/4)\ L_d}{2\pi a}\sqrt{\frac{\rho}{2Z_0\sigma_z^3}} \tag{23}$$

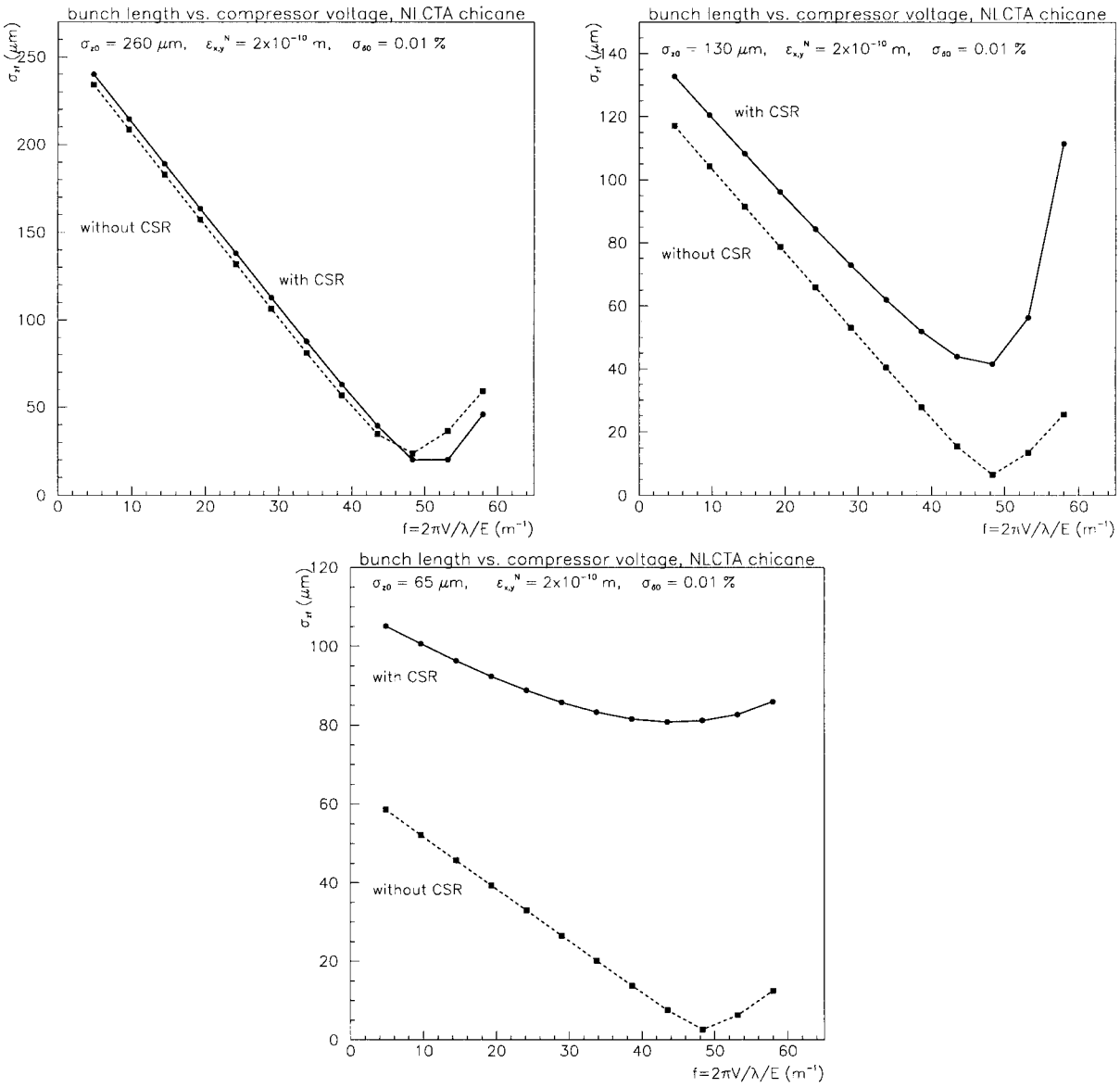

Figure 15: Final bunch length versus compressor rf voltage for beam transport through the NLCTA chicane, with and without coherent synchrotron radiation, for three different initial bunch lengths σ_{zi}. Straight horizontal lines represent the estimates of Eq. (18). Left: $\sigma_{zi} = 260$ μm, center: $\sigma_{zi} = 130$ μm, right: $\sigma_{zi} = 65$ μm.

magnet	σ_z	δ_{CSR}	$h_c\ (=2a_c)$	a†	$\delta^{(a)}_{CSR}$	$\delta^{(a)}_{RW}$	$\delta^{(a)\ *}_{geom}$
bend 1	260 μm	0.08%	9.3 mm	8 mm	0.08%	2×10^{-6}	0
bend 2	211 μm	0.13%	8.1 mm	8 mm	0.12%	3×10^{-6}	0
bend 3	101 μm	0.33%	4.9 mm	**1.5 mm**	0.11%	5×10^{-5}	0.16%
bend 4	59 μm	0.76%	3.5 mm	**1.0 mm**	0.20%	2×10^{-4}	0.35%

Table 3: Summary of energy spread due to CSR and wakefields in the four bends of the chicane, for a bunch compression to $\sigma_{zf} = 60$ μm. Quantities with superindex (a) assume a reduced aperture in the last two bending magnets (see also Table 3).
† reduced half aperture for last two bends; * without taper

where a denotes the *half* aperture ($a = h/2$), Z_0 the vacuum impedance ($Z_0 = 377\ \Omega$), $\Gamma(3/4) \approx 1.23$, L the bending-magnet length ($L = 2$ m), and ρ here is the resistivity of the beam pipe ($\rho \approx 10^{-7}\ \Omega$ m, if we pessimistically assume that the shield is made from Fe). The induced rms energy spread is comparable to the average energy loss: $\delta_{rms} \approx 1.1\delta_{ave}$.

In addition, if the beam is off-set from the center by y, the transverse dipole wakefield exerts a kick

$$< \Delta y' > \approx \frac{2Nr_e}{\gamma} \frac{L_d \Gamma(1/4)}{\pi a^3} \sqrt{\frac{\rho}{2Z_0\sigma_z}}\, \Delta y \tag{24}$$

where $\Gamma(1/4) \approx 3.63$.

Finally, the beam also loses energy due to the geometric wakefield, which for an untapered transition between radius b and radius a reads:

$$\delta_{ave} \approx \frac{2Nr_e}{\gamma} \frac{1}{\sqrt{\pi}\sigma_z} \ln\left(\frac{b}{a}\right) \tag{25}$$

and the rms energy spread is again similar to the average energy loss, $\delta_{rms} \approx 0.4\ \delta_{ave}$.

Tables 3 and 4 summarize the energy spread and emittance growth induced by coherent synchrotron radiation and by longitudinal wakefields. The tables show that a smaller aperture in the last two bending magnets can reduce the energy spread due to CSR by about a factor of three, with an accompanying reduction in the emittance growth. Table 4 also shows that, if the aperture restriction is not tapered, this improvement is almost nulled by geometric wakefields, and that, for reasonably centered beams, the dipole resistive-wall wakefield is insignificant.

7 Structure Alignment

To confirm that the required structure alignment tolerances for the NLCTA FEL are not too tight, a simulation with the code MAD was performed. Here, the two structures accelerating the beam from 6 MeV to 100 MeV were displaced together by various amplitudes y, and the resulting emittance at the end of the chicane was determined by multiparticle tracking. The results of this simulation study are compiled in Table 5. Note that the table does not show the emittance growth but the total final emittance, starting with $\gamma\epsilon_x \sim 1.5$ μm.

magnet	$\Delta\epsilon_{CSR}$	$\Delta\epsilon_{CSR}^{(a)}$ †	$\Delta\epsilon_{RW}^{(a)}$ †	$\Delta\epsilon_{geom}^{(a)}$ * †	$\Delta y'/\sigma_{y'}\vert_{RW}$ *
bend 1	0	0	0	0	0
bend 2	0	0	0	0	0
bend 3	1.95 μm	0.65 μm	0	0.09 μm	0.01
bend 4	0.27 μm	0.08 μm	0	0.14 μm	0.06

Table 4: Summary of emittance growth due to CSR and wakefields in the four bends of the chicane, for a bunch compression to $\sigma_{zf} = 60$ μm. Quantities with superindex (a) assume a reduced aperture in the last two bending magnets (see also Table 3).
* without taper; † scaled from δ_{CSR} (Table 3) and ϵ_{CSR}; * for $\Delta y = 100$ μm

Δy [μm]	$\gamma\epsilon_y$ [mm mrad]
20	1.49
200	1.61
2000	8.11

Table 5: Final vertical emittance for various vertical displacements of the two accelerating sections upstream of the chicane.

The table suggests that the alignment tolerances are not particularly tight. Displacements by up to a few hundred microns do not lead to significant additional emittance growth.

8 Conclusions

In this report, I have summarized the beam dynamics studies regarding a possible bunch compression in the NLCTA FEL. The bunch-length compression from 260 μm to 60–120 μm rms with the existing chicane was shown to be straightforward. I have demonstrated that most of the other desired beam parameters are easily achieved as well. There is only one exception to this positive finding: the horizontal emittance. The existing theories of coherent synchrotron radiation predict the projected horizontal emittance to blow up substantially in the NLCTA chicane.

It must be noted that the present theories of coherent synchrotron radiation have several shortcomings, none the least of which is that, in the treatment of the energy loss, they ignore the transverse beam dimensions, and that they, thus, may widely overestimate the induced energy spread and the emittance growth. However, assuming the present theory is applicable, barely acceptable emittance values can be achieved when the half aperture in the last two bending magnets is reduced from 8 to 1–1.5 mm. This represents a workable and, perhaps, attractive solution, but our present incliniation is to bypass the NLCTA chicane altogether and to generate the short bunches with an X-band rf gun.

Even so, the NLCTA chicane would offer the unique possibility to study the emittance growth arising from coherent synchrotron radiation for very short bunches. This will be of considerable interest to many future projects, in particular to the LCLS.

References

[1] K. Oide, "Synchrotron-Radiation Limit on the Focusing of Electron Beams", Phys. Rev. Lett. **61**, 15 p. 1713 (1988).

[2] NLC Test Accelerator, SLAC-411 (1993).

[3] J. Arthur, G. Materlik, R. Tatchyn, H. Winick, "The LCLS: A Fourth Generation Light Source Using the SLAC Linac", Rev. Sci. Intrum. 66 p. 1987 (1995).

[4] C. Adolphsen, T. Lavine, R. Miller, H.-D. Nuhn, R. Ruth, J. Schmerge, J. Wang, H. Winick, D. Yeremian, F. Zimmermann, "The NLCTA as an FEL Driver – A Preliminary Study", report in preparation (1997).

[5] R. Ruth, private communication (1997).

[6] K. L. Brown, "A First- and Second-Order Matrix Theory for the Design of Beam Transport Systems and Charged Particle Spectrometers", *SLAC*-**75** (1982).

[7] The simulation code LITRACK was written by Bane.

[8] H. Grote and C. Iselin, CERN Report No. CERN/SL/90-13 (1990).

[9] Ya.S. Derbenev, J. Rossbach, E.L. Saldin, and V.D. Shiltsev, "Microbunch Radiative Tail-Head Interaction", DESY TESLA-FEL 95-05 (1995).

[10] J.B. Murphy, S. Krinsky, R.L. Gluckstern, "Longitudinal Wake Field for an Electron Moving on a Circular Orbit", BNL-63090 (1996).

[11] E.L. Saldin, E.A. Schneidmiller, M.V. Yurkov, "On the Coherent Radiation of an Electron Bunch Moving in an Arc of a Circle", DESY TESLA-FEL 96-14 (1996).

[12] Ya.S. Derbenev and V.D. Shiltsev, "Transverse Effects of Microbunch Radiative Interaction", SLAC-PUB-7181 (1996).

[13] M. Dohlus and T. Limberg, "Emittance Growth due to Wake Fields on Curved Bunch Trajectories", DESY internal report (1996).

[14] R. Talman, Phys. Rev. Lett. **56**, 1429 (1986).

[15] A. Piwinski, CERN Report No. CERN/LEP-TH/85-43 (1985).

[16] B. Carlsten and T. Raubenheimer, Phys. Rev. E 51, no. 2, 0. 1453 (1995).

[17] P. Emma, private communication (1996).

[18] R.L. Warnock, "Shielded Coherent Synchrotron Radiation and Its Possible Effect in the Next Linear Collider", Proc. IEEE PAC 1991 San Francisco and SLAC-PUB-5523 (1991).

[19] R. Warnock, private communication (1996).

[20] S.A. Heifets and S.A. Kheifets, "Coupling Impedance in Modern Accelerators", Rev. Mod. Phys., Vol. 63, No. 3 (1991).

[21] L. Palumbo, "Analytical Calculation of the Impedance of a Discontinuity", Particle Accelerators 25, pp. 201–216 (1990).

[22] T. Raubenheimer and F. Zimmermann, "Longitudinal Wake Fields and Chromatic Spot-Size Dilution in the NLC Final Focus", NLC Note 23 (1996).